Solving a class of biological HIV infection model of latently infected cells using heuristic approach

Yolanda Guerrero Sanchez[1], Muhammad Umar[2], Zulqurnain Sabir[3], Juan L.G. Guirao[4,*], Muhammad Asif Zahoor Raja[5]

[1]Department of Dermatology, Stomatology, Radiology and Physical Medicine, University of Murcia, Spain

Email: yolanda.guerreros@um.es

[2]Department of Mathematics and Statistics, Hazara University, Mansehra, Pakistan

Emails: umar_maths@hu.edu.pk, humar922015@gmail.com

[3,*]Department of Mathematics and Statistics, Hazara University, Mansehra, Pakistan

Emails: zulqurnain_maths@hu.edu.pk, zulqurnainsabir@gmail.com, +923335868270

[4]Department of Applied Mathematics and Statistics, Technical University of Cartagena, Hospital de Marina 30203-Cartagena, Spain

Email: juan.garcia@upct.es

[5]Department of Electrical Engineering, COMSATS Institute of Information Technology, Attock, Pakistan

Email: Muhammad.asif@ciit-attock.edu.pk

Abstract:

The intension of the recent study is to solve a class of biological nonlinear HIV infection model of latently infected CD4+T cells using feed-forward artificial neural networks, optimized with global search method, i.e. particle swarm optimization (PSO) and quick local search method, i.e. interior-point algorithms (IPA). An unsupervised error function is made based on the differential equations and initial conditions of the infection model of latently infected CD4+T cells. For the correctness and reliability of the present scheme, comparison is made of the present results with the Adams numerical results. Moreover, statistical measures based on mean absolute deviation, root mean square error and Theil's inequality coefficient demonstrates the effectiveness, applicability and convergence of the designed scheme.

Keywords: HIV infection, particle swarm, hybrid approach, interior-point algorithm, artificial neural networks, statistical analysis.

1. Introduction

HIV is known as a dangerous virus that spreads through body fluids and attacks immune system of the body. It destroys and kills many of the CD4 cells (T cells), so the body fails to fight off disease and infections, due to this, the number of CD4 cells is reduced in the body. The damage in the immune system makes the body harder to fight against infections and other diseases. Many serious/global diseases like cancer, HIV/AIDS and opportunistic infections get the advantage of the weak body's immune system. The huge amount has been spent for the treatment of these kinds of diseases every year, but no cure is found yet [1].

Many mathematical models have been suggested to understand the dynamics of HIV, anti-retroviral response and disease progression, etc. [2-4]. Research community shows that a substantial proportion of T cells are diseased by the virus and they presented a model using the HIV infection in 1989. The main features of this model have three variables: infected cells, the

population sizes of uninfected cells and free virus particles. Computational and mathematical models of the human immune together with the viral infection and experimental measurements have produced important visions into HIV-1 pathogenesis and has improved development to understand the HIV-1 infection.

To present the model, it is supposed that infected CD4+ T-cells [5-6] are either latent or active. Due to infection, most of the healthy T-cells lost, one fraction of these cells becomes productively infected, active or latent. Both infected cells classes are assumed to expire with the disturbance of exponentially waiting time [9]. For the simple mass-action infection term, the following system of nonlinear differential equations is studied [10]:

$$\begin{cases} \dfrac{dx}{dt} = \mu - dx - \alpha xv, & x(0) = S_1, \\ \dfrac{dw}{dt} = -(q-1)\alpha xv - ew - \lambda w, & w(0) = S_2, \\ \dfrac{dy}{dt} = \lambda w - ay + q\alpha xv, & y(0) = S_3, \\ \dfrac{dv}{dt} = -uv + ky, & v(0) = S_4. \end{cases} \tag{1}$$

Where S_1, S_2, S_3, S_4 and λ are constants. α and μ are the infected and uninfected CD4+T cells. d and a are the death rate of host cells and HIV-1infected cells, e is the infection rate by recombinant, k is the HIV-1 production rate by cells, u is the pathogen removed rate and q is the removal rate of recombinant.

To solve the biological model (1) is not easy due to the nonlinearity. However, only a few techniques are available in the literature to solve the biological nonlinear HIV infection model of latently infected CD4+T cells. Few of them are Adomian decomposition method [10], finite difference scheme [11], Legendre wavelet method [12], sequential Bayesian analysis approach [13], homotopy analysis method [14], Bessel collocation technique [15] and method of differential transformation [16].

All the above mention techniques have their individual merits/demerits, advantages/disadvantages, whereas, stochastic numerical solvers based on artificial neural networks (ANNs) are found to be efficient, precise and consistent for solving competently optimization models arising in various fields [17-21]. Some recent applications of stochastic solvers are nonlinear prey-predator models [22], nonlinear Troesch's problem arising in plasma physics [23], cell biology [24], inverse kinematics problems [25], thin-film flow [26], uncertainties in computational mechanics [27], power [28], fuzzy differential equations [29], nanofluidic problems [30], nonlinear singular Thomas-Fermi systems [31], doubly-singular systems [32], heat conduction model of human head [33], transistor-level uncertainty quantification [34], control system [35] and energy [36].

The aim of the present work is to solve the HIV model (1) numerically by using the ANNs optimized by particle swarm optimization (PSO), interior-point algorithm (IPA) and the hybrid combination of PSO-IPA. Some prime features of the present scheme are as follows:

- Investigation and exploitation of ANNs constructed by stochastic numerical solvers to discover the precise and consistent results for the nonlinear biological model.

- The present approach is applied effectively to solve the nonlinear biological model. The present results of the designed scheme are compared with the Adams numerical results that proves the worth of the scheme.
- Authentication of the scheme is certified through statistics based on a number of performance monitory matrices on minimum, maximum, median and semi interquartile ranges.

2. Design Methodology

The proposed structure of the present scheme of the model (1) is divided into two portions. By introducing an error based fitness function and the combination of PSO-IPA along with the pseudocode is discussed in detail, while and the graphical abstract of PSO-IPA is plotted in Fig. 1.

2.1 ANN Modeling

The formulation of the model (1) with feed-forward ANNs in the form of $x(t), w(t), y(t)$ and v(t), as well as, their respective *n* derivatives are given as:

$$\left[\hat{x}(t), \hat{w}(t), \hat{y}(t), \hat{v}(t)\right] = \begin{bmatrix} \sum_{i=1}^{m} \varphi_{x,i} h(w_{x,i} t + b_{x,i}), \sum_{i=1}^{m} \varphi_{w,i} h(w_{w,i} t + b_{w,i}), \\ \sum_{i=1}^{m} \varphi_{y,i} h(w_{y,i} t + b_{y,i}), \sum_{i=1}^{m} \varphi_{v,i} h(w_{v,i} t + b_{v,i}) \end{bmatrix}, \tag{2}$$

$$\left[\hat{x}^{(n)}, \hat{w}^{(n)}, \hat{y}^{(n)}, \hat{v}^{(n)}\right] = \begin{bmatrix} \sum_{i=1}^{m} \varphi_{x,i} h^{(n)}(w_{x,i} t + b_{x,i}), \sum_{i=1}^{m} \varphi_{w,i} h^{(n)}(I_{w,i} t + b_{w,i}), \\ \sum_{i=1}^{m} \varphi_{y,i} h^{(n)}(I_{y,i} t + b_{y,i}), \sum_{i=1}^{m} \varphi_{v,i} h^{(n)}(I_{v,i} t + b_{v,i}) \end{bmatrix}.$$

Where $\boldsymbol{W}$ is the unknown weight vector and defined as:

$\boldsymbol{W} = [\boldsymbol{W}_T, \boldsymbol{W}_I, \boldsymbol{W}_V]$, for $\boldsymbol{W}_x = [\boldsymbol{\varphi}_x, \boldsymbol{w}_x, \boldsymbol{b}_x]$, $\boldsymbol{W}_w = [\boldsymbol{\varphi}_w, \boldsymbol{w}_w, \boldsymbol{b}_w]$, $\boldsymbol{W}_y = [\boldsymbol{\varphi}_y, \boldsymbol{w}_y, \boldsymbol{b}_y]$ and $\boldsymbol{W}_v = [\boldsymbol{\varphi}_v, \boldsymbol{w}_v, \boldsymbol{b}_v]$. The weight vector $\boldsymbol{W}$ is given as:

$\boldsymbol{\varphi}_x = [\varphi_{x,1}, \varphi_{x,2}, ..., \varphi_{x,m}], \boldsymbol{\varphi}_w = [\varphi_{w,1}, \varphi_{w,2}, ..., \varphi_{w,m}], \boldsymbol{\varphi}_y = [\varphi_{y,1}, \varphi_{y,2}, ..., \varphi_{y,m}], \boldsymbol{\varphi}_v = [\varphi_{v,1}, \varphi_{v,2}, ..., \varphi_{v,m}],$

$\boldsymbol{w}_x = [w_{x,1}, w_{x,2}, ..., w_{x,m}], \boldsymbol{w}_w = [w_{w,1}, w_{w,2}, ..., w_{w,m}], \boldsymbol{w}_y = [w_{y,1}, w_{y,2}, ..., w_{y,m}], \boldsymbol{w}_v = [w_{v,1}, w_{v,2}, ..., w_{v,m}],$

$\boldsymbol{b}_x = [b_{x,1}, b_{x,2}, ..., b_{x,m}], \boldsymbol{b}_w = [b_{w,1}, b_{w,2}, ..., b_{w,m}], \boldsymbol{b}_y = [b_{y,1}, b_{y,2}, ..., b_{y,m}], \boldsymbol{b}_v = [b_{v,1}, b_{v,2}, b_{v,3}, ..., b_{v,m}].$

Using the log-sigmoid activation function $\frac{1}{1+\exp(-t)}$. The updated form of the network (2) becomes as:

$$\left[\hat{x}(t),\hat{w}(t),\hat{y}(t),\hat{v}(t)\right]=\begin{bmatrix}\sum_{i=1}^{m}\frac{\varphi_{x,i}}{1+e^{-\left(w_{x,i}t+b_{x,i}\right)}},\ \sum_{i=1}^{m}\frac{\varphi_{w,i}}{1+e^{-\left(w_{w,i}t+b_{w,i}\right)}},\\ \sum_{i=1}^{m}\frac{\varphi_{y,i}}{1+e^{-\left(w_{y,i}t+b_{y,i}\right)}},\sum_{i=1}^{m}\frac{\varphi_{v,i}}{1+e^{-\left(w_{v,i}t+b_{v,i}\right)}}\end{bmatrix},$$

$$\left[\hat{x}'(t),\hat{w}'(t),\hat{y}'(t),\hat{v}'(t)\right]=\begin{bmatrix}\sum_{i=1}^{m}\frac{\varphi_{x,i}w_{x,i}e^{-\left(w_{x,i}t+b_{x,i}\right)}}{\left(1+e^{-\left(w_{x,i}t+b_{x,i}\right)}\right)^2},\ \sum_{i=1}^{m}\frac{\varphi_{w,i}w_{I,i}e^{-\left(w_{w,i}t+b_{w,i}\right)}}{\left(1+e^{-\left(w_{w,i}t+b_{w,i}\right)}\right)^2},\\ \sum_{i=1}^{m}\frac{\varphi_{y,i}w_{y,i}e^{-\left(w_{y,i}t+b_{y,i}\right)}}{\left(1+e^{-\left(w_{y,i}t+b_{y,i}\right)}\right)^2},\sum_{i=1}^{m}\frac{\varphi_{v,i}w_{I,i}e^{-\left(w_{v,i}t+b_{v,i}\right)}}{\left(1+e^{-\left(w_{v,i}t+b_{v,i}\right)}\right)^2}\end{bmatrix}. \quad \textbf{(3)}$$

Using the model (3), the fitness/error function is written as:

$$\xi=\xi_1+\xi_2+\xi_3+\xi_4+\xi_5, \quad \textbf{(4)}$$

$$\xi_1=\frac{1}{N}\sum_{m=1}^{N}\left(\frac{dx_m}{dt}-\mu+dx_m+\alpha x_m v_m\right)^2, \quad \textbf{(5)}$$

$$\xi_2=\frac{1}{N}\sum_{m=1}^{N}\left(\frac{dw_m}{dt}+(q-1)\alpha x_m v_m+ew_m+\lambda w_m\right)^2, \quad \textbf{(6)}$$

$$\xi_3=\frac{1}{N}\sum_{m=1}^{N}\left(\frac{dy_m}{dt}-\lambda w_m+ay_m-q\alpha x_m v_m\right)^2, \quad \textbf{(7)}$$

$$\xi_4=\frac{1}{N}\sum_{m=1}^{N}\left(\frac{dv_m}{dt}+u_m v_m-ky_m\right)^2, \quad \textbf{(8)}$$

$$\xi_5=\frac{1}{3}\left(\left(\hat{x}_0-S_1\right)^2+\left(\hat{w}_0-S_2\right)^2+\left(\hat{y}_0-S_3\right)^2+\left(\hat{v}_0-S_4\right)^2\right). \quad \textbf{(9)}$$

Where $N=\frac{1}{h}$, $\hat{x}_m=\hat{x}\left(t_m\right)$, $\hat{w}_m=\hat{w}\left(t_m\right)$, $\hat{y}_m=\hat{y}\left(t_m\right)$, $\hat{v}_m=\hat{v}\left(t_m\right)$, $t_m=mh$, ξ_1, ξ_2, ξ_3 and ξ_4 are the fitness functions associated with differential equations of the model (1), whereas, ξ_5 is the error function related to the initial condition of model (1). The solution can be attained from the available weights, and the fitness function using $\xi\to 0$. Then the approximate solutions $\left[\hat{x}(t),\hat{w}(t),\hat{y}(t),\hat{v}(t)\right]$ become identical, *i.e.*, $[\hat{x}(t)\to x(t)]$, $[\hat{w}(t)\to w(t)]$, $[\hat{y}(t)\to y(t)]$ and $[\hat{v}(t)\to v(t)]$.

2.2. Optimization procedure: PSO-IPA

For optimization of ANNs, hybrid-computing framework based on PSO-IPA is used.

Particle Swarm Optimization: It is a heuristic global search optimization process, suggested by Eberhart and Kennedy in the last decade of the nineteen century. PSO is replacement of genetic algorithms [37] and used as an optimization procedure because of easy implementation and short memory requirements [38]. PSO is applied to the collaborative swarm routine of fish schooling and birds flocking [39]. Some recent applications of PSO are multicast routing problem in communication networks [40], solar photovoltaic system [41], clustering high-dimensional data [42], for multilevel thresholding [43], for energy resource scheduling considering vehicle-to-grid [44], optimization for humanoid robots [45], collective robotic search applications [46] and gene selection in cancer classification [47].

In the theory of search space, every single candidate solution for an optimization model is denoted as a particle. In the algorithm of PSO, the problem is explored by casually generated particles to form a swarm. For optimal performance of the procedure, initial swarms spread in the grander size. To initialize the parameters runs in the PSO, the algorithm provides iteratively optimal solutions. The position and velocity in the swarm are $\boldsymbol{P}_{LB}^{a-1}$ and $\boldsymbol{P}_{GB}^{a-1}$. The standard continuous form for position and velocity is shown as:

$$\boldsymbol{X}_j^a = \boldsymbol{X}_j^{a-1} + \boldsymbol{V}_j^{a-1} \tag{10}$$

$$\boldsymbol{V}_j^a = \omega \boldsymbol{V}_j^{a-1} + a_1 \boldsymbol{r}_1 (\boldsymbol{P}_{LB}^{a-1} - \boldsymbol{X}_j^{a-1}) + a_2 \boldsymbol{r}_2 (\boldsymbol{P}_{GB}^{a-1} - \boldsymbol{X}_j^{a-1}) \tag{11}$$

Where the vector $\mathbf{X}_j$ and $\boldsymbol{V}_j$ represents the j^{th} swarm particle and the velocity vector respectively. The random vectors are $\boldsymbol{r}_1$ and $\boldsymbol{r}_2$, $\omega \in [0,1]$ shows the inertia weight, whereas, a_1 and a_2 are the acceleration constants. The elements in the velocity vector lie in $[-v_{max}, v_{max}]$, where v_{max} shows maximum velocity. The performance of the algorithm is stopped when the predefined number of flights obtained.

Interior-point algorithm: It is one of the efficient, rapid and fast local search optimization algorithm. IPA works to solve both type of problems constrained and unconstrained. In recent years, IPA is used in many applications e.g., large-scale optimal power flow problems [48], simulation of aircraft parts riveting [49], simulation of viscoplastic fluid flows [50], reliable treatment of economic load dispatch problem [51], for non-smooth contact dynamics [52] and non-smooth contact dynamics. In the present work, hybrid of PSO-IPA is used to find the designed variables for solving the model (1).

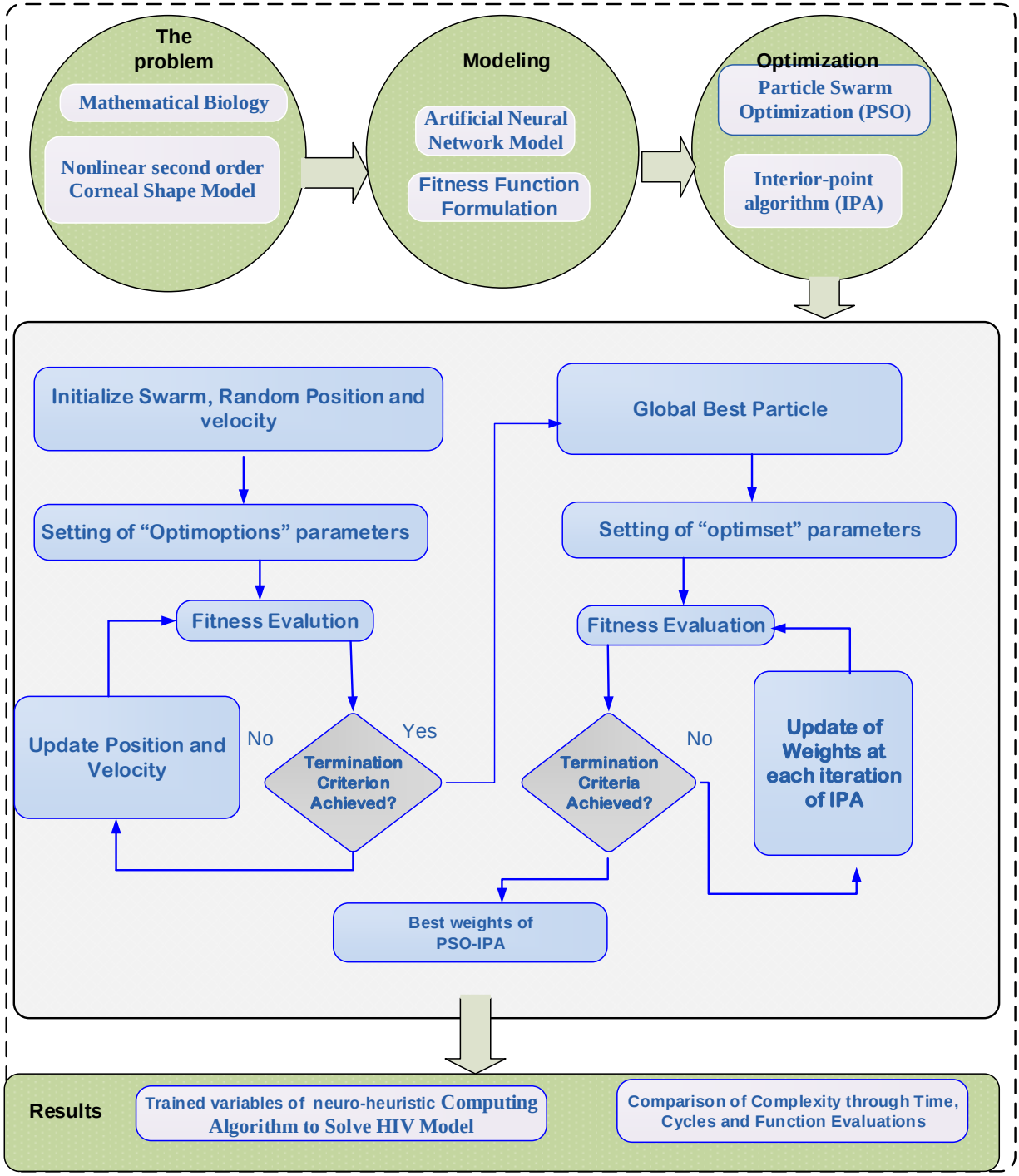

Figure 1: Graphical illustration of present scheme for HIV model

3. Performance indices

The performance measures for the HIV model (1) based on mean absolute deviation (MAD), root mean square error (RMSE) and Theil's inequality coefficient (TIC). The mathematical form of MAD, RMSE and TIC is given as:

$$\left[MAD_x, MAD_w, MAD_y, MAD_v\right] = \begin{bmatrix} \frac{1}{m}\sum_{i=1}^{m}\left|x_i - \hat{x}_i\right|, \frac{1}{m}\sum_{i=1}^{m}\left|w_i - \hat{w}_i\right|, \\ \frac{1}{m}\sum_{i=1}^{m}\left|y_i - \hat{y}_i\right|, \frac{1}{m}\sum_{i=1}^{m}\left|v_i - \hat{v}_i\right| \end{bmatrix}, \tag{12}$$

$$[\mathrm{RMSE}_x, \mathrm{RMSE}_w, \mathrm{RMSE}_y, \mathrm{RMSE}_v] = \begin{bmatrix} \sqrt{\frac{1}{m}\sum_{i=1}^{m}\left(x_i - \hat{x}_i\right)^2}, \sqrt{\frac{1}{m}\sum_{i=1}^{m}\left(w_i - \hat{w}_i\right)^2} \\ \sqrt{\frac{1}{m}\sum_{i=1}^{m}\left(y_i - \hat{y}_i\right)^2}, \sqrt{\frac{1}{m}\sum_{i=1}^{m}\left(v_i - \hat{v}_i\right)^2} \end{bmatrix}., \tag{13}$$

$$[\mathrm{TIC}_x, \mathrm{TIC}_w, \mathrm{TIC}_y, \mathrm{TIC}_v] = \begin{pmatrix} \frac{\sqrt{\frac{1}{m}\sum_{i=1}^{m}\left(x_i - \hat{x}_i\right)^2}}{\left(\sqrt{\frac{1}{m}\sum_{i=1}^{m}x_i^2} + \sqrt{\frac{1}{m}\sum_{i=1}^{m}\hat{x}_i^2}\right)}, \frac{\sqrt{\frac{1}{m}\sum_{i=1}^{m}\left(w_i - \hat{w}_i\right)^2}}{\left(\sqrt{\frac{1}{m}\sum_{i=1}^{m}w_i^2} + \sqrt{\frac{1}{m}\sum_{i=1}^{m}\hat{w}_i^2}\right)}, \\ \frac{\sqrt{\frac{1}{m}\sum_{i=1}^{m}\left(y_i - \hat{y}_i\right)^2}}{\left(\sqrt{\frac{1}{m}\sum_{i=1}^{m}y_i^2} + \sqrt{\frac{1}{m}\sum_{i=1}^{m}\hat{y}_i^2}\right)}, \frac{\sqrt{\frac{1}{m}\sum_{i=1}^{m}\left(v_i - \hat{v}_i\right)^2}}{\left(\sqrt{\frac{1}{m}\sum_{i=1}^{m}v_i^2} + \sqrt{\frac{1}{m}\sum_{i=1}^{m}\hat{v}_i^2}\right)} \end{pmatrix}. \tag{14}$$

Table 1: Pseudo code using GA-SQP

Start of PSO

Inputs:

The chromosome with same number of entries of the network

$$\boldsymbol{W} = [\boldsymbol{W}_x, \boldsymbol{W}_w, \boldsymbol{W}_y, \boldsymbol{W}_v] = [(\boldsymbol{\varphi}_x, \boldsymbol{w}_x, \boldsymbol{b}_x), (\boldsymbol{\varphi}_w, \boldsymbol{w}_w, \boldsymbol{b}_w), (\boldsymbol{\varphi}_y, \boldsymbol{w}_y, \boldsymbol{b}_y), (\boldsymbol{\varphi}_v, \boldsymbol{w}_v, \boldsymbol{b}_v)]$$

$$\boldsymbol{\varphi}_x = [\varphi_{x,1}, \varphi_{x,2}, ..., \varphi_{x,m}], \boldsymbol{\varphi}_w = [\varphi_{w,1}, \varphi_{w,2}, ..., \varphi_{w,m}], \boldsymbol{\varphi}_y = [\varphi_{y,1}, \varphi_{y,2}, ..., \varphi_{y,m}], \boldsymbol{\varphi}_v = [\varphi_{v,1}, \varphi_{v,2}, ..., \varphi_{v,m}],$$

$$\boldsymbol{w}_x = [w_{x,1}, w_{x,2}, ..., w_{x,m}], \boldsymbol{w}_w = [w_{w,1}, w_{w,2}, ..., w_{w,m}], \boldsymbol{w}_y = [w_{y,1}, w_{y,2}, ..., w_{y,m}], \boldsymbol{w}_v = [w_{v,1}, w_{v,2}, ..., w_{v,m}],$$

$$\boldsymbol{b}_x = [b_{x,1}, b_{x,2}, ..., b_{x,m}], \boldsymbol{b}_w = [b_{w,1}, b_{w,2}, ..., b_{w,m}], \boldsymbol{b}_y = [b_{y,1}, b_{y,2}, ..., b_{y,m}], \boldsymbol{b}_v = [b_{v,1}, b_{v,2}, b_{v,3}, ..., b_{v,m}].$$

Population: The set of chromosomes is

$$\boldsymbol{P} = [(\boldsymbol{W}_{x1}, \boldsymbol{W}_{x2}, ..., \boldsymbol{W}_{xn}), (\boldsymbol{W}_{w1}, \boldsymbol{W}_{w2}, ..., \boldsymbol{W}_{wn}), (\boldsymbol{W}_{y1}, \boldsymbol{W}_{y2}, ..., \boldsymbol{W}_{yn}), (\boldsymbol{W}_{v1}, \boldsymbol{W}_{v2}, ..., \boldsymbol{W}_{vn})]$$

$$[\boldsymbol{W}_{xi}, \boldsymbol{W}_{wi}, \boldsymbol{W}_{yi}, \boldsymbol{W}_{vi}] = [(\boldsymbol{\varphi}_{xi}, \boldsymbol{w}_{xi}, \boldsymbol{b}_{xi}), (\boldsymbol{\varphi}_{wi}, \boldsymbol{w}_{wi}, \boldsymbol{b}_{wi}), (\boldsymbol{\varphi}_{yi}, \boldsymbol{w}_{yi}, \boldsymbol{b}_{yi}), (\boldsymbol{\varphi}_{vi}, \boldsymbol{w}_{vi}, \boldsymbol{b}_{vi})]$$

Output: Global best values of PSO is denoted as $\boldsymbol{W}_{\mathbf{B:PSO}}$

Initialization

Produce $\boldsymbol{W}$ of real numbers to signify a chromosome to make an Initial $\boldsymbol{P}$. Set the practice of Generation and declarations values of "PSO" and "gaoptimset" measures

Calculations of Fitness

To calculate the fitness ζ using Eq.(4)

Ranking

Each $\boldsymbol{W}$ of $\boldsymbol{P}$ ranked through brilliance of the fitness rate.

Stopping criteria

Stop the optimization procedure for any of the following

- Level of fitness achieved
- Number of preferred flights/cycles performed

Renewal

Call the position using equations (10) and velocity using equation (11).

Improvement

Repeat the algorithm until the whole number of flights achieved

Storage

Store the best fitness values and signify it the global best particle.

End of PSO algorithms

PSO-IPA Procedure Start

Inputs

$\boldsymbol{W}_{B:GA}$

Output

The best vector of PSO:IPA is $\boldsymbol{W}_{\mathbf{PSO:IPA}}$

Initialize

Use $\boldsymbol{W}_{B:GA}$ as a start point

Decelerations and bounded based on "optimset" and "fmincon" routines,

Termination

When any of the value meet, stop the algorithm
'Fitness limit' = '$\zeta \leq 10^{-18}$', 'total Iterations' = '1000', 'TolFun' ≤ '10^{-18}', 'TolX' ≤ '10^{-18}', 'TolCon' ≤ '10^{-20}', 'MaxFunEvals' ≤ '250000'

While (Terminate)

Fitness calculation

Using Eqs (4-9), find the fitness ζ

Adjustments

Invoking 'fmincon' routine using algorithm 'IPA' to adjust $\boldsymbol{W}$. Go to the step of fitness with updated $\boldsymbol{W}$

End

Save the final adaptive weights $W_{PSO\text{-}IPA}$ *and* ζ, iterations, time and function count for the current run.

PSO-IPA Procedure End

3. Results and discussion

The detailed result and discussion of the model (1) is presented in this section by taking five number of neurons. The comparison of present results with the Adams numerical results shows the exactness and correctness of the proposed scheme. Moreover, statistical results are performed to check the precision and accuracy of the present technique.

3.1 HIV infection model of latently infected cells

The updated form of the model (1) by taking the values of
$S_1 = 7,\ S_2 = 2, S_3 = 1, S_4 = 4, \alpha = 0.04, \mu = 0.4, d = 0.01, e = 0.1, a = 0.2,\ k = 0.6,\ u = 0.03,\ q = 0.8, \lambda = 0.3.$

$$\begin{cases} \dfrac{dx}{dt} = 0.4 - 0.01x - 0.04xv, & x(0) = 7 \\ \dfrac{dw}{dt} = 0.008xv - 0.4w, & w(0) = 2 \\ \dfrac{dy}{dt} = 0.3w - 0.2y + 0.032xv, & y(0) = 1 \\ \dfrac{dv}{dt} = -uv + 0.6y, & v(0) = 1 \end{cases} \tag{15}$$

The error/fitness function of the model (15) is written as:

$$\zeta = \frac{1}{N}\sum_{m=1}^{N}\left(\begin{array}{l}\left[\frac{dx_m}{dt} - 0.4 + 0.01 * x_m + 0.04 * x_m v_m\right]^2 + \left[\frac{dw_m}{dt} - 0.008 * x_m v_m + 0.4 * v_m\right]^2 \\ + \left[\frac{dy_m}{dt} - 0.3 * w_m + 0.2 * y_m - 0.032 * x_m * v_m\right]^2 + \left[\frac{dv_m}{dt} + u_m v_m - 0.6 * y_m\right]^2\end{array}\right) + \frac{1}{4}\left(\left(\hat{x}_0 - 7\right)^2 + \left(\hat{w}_0 - 2\right)^2 + \left(\hat{y}_0 - 1\right)^2 + \left(\hat{v}_0 - 1\right)^2\right), \quad \textbf{(16)}$$

Optimization of all variants of the model (1) is supported by the combination of PSO-IPA for hundred numbers of runs to achieve the network parameters. The weights set is provided to obtain the approximate solution for the model (1). The mathematical form of the approximate solution becomes as:

$$\hat{x}(t) = \frac{0.1615}{1+e^{-(-4.5041t-2.7123)}} + \frac{1.4934}{1+e^{-(-1.3373t-0.5227)}} + \frac{6.8018}{1+e^{-(-3.0218t+6.9131)}} + \frac{-0.3605}{1+e^{-(0.2689t-1.1503)}} + \frac{-2.6949}{1+e^{-(1.1514t-2.1777)}} \quad \textbf{(17)}$$

$$\hat{w}(t) = \frac{1.1743}{1+e^{-(-0.4197t-0.9589)}} + \frac{2.3207}{1+e^{-(-0.8906t-2.1978)}} + \frac{0.6713}{1+e^{-(-1.7834t-8.4626)}} + \frac{5.8251}{1+e^{-(0.0674t+1.0848)}} + \frac{-3.9497}{1+e^{-(0.4770t+1.0307)}} \quad \textbf{(18)}$$

$$\hat{y}(t) = \frac{6.1731}{1+e^{-(0.4578t-3.9406)}} + \frac{4.0619}{1+e^{-(1.3612t+1.8178)}} + \frac{0.1770}{1+e^{-(0.5817t-0.6665)}} + \frac{-3.5977}{1+e^{-(-0.8200t+1.0544)}} + \frac{-0.1097}{1+e^{-(2.4635t-3.2401)}} \quad \textbf{(19)}$$

$$\hat{v}(t) = \frac{1.5157}{1+e^{-(-1.0591t-5.8109)}} + \frac{-0.3853}{1+e^{-(-2.7099t+1.5490)}} + \frac{6.7429}{1+e^{-(0.0742t+0.1897)}} + \frac{5.6749}{1+e^{-(0.9777t-2.1071)}} + \frac{0.5811}{1+e^{-(-3.2119t-4.3057)}} \quad \textbf{(20)}$$

The graphic illustration using GA-IPA for all the parameters of example 1 is narrated in Figs 2 to 7 by taking 5 number of neurons. The set of weights for the parameters $x(t)$, $w(t)$, $y(t)$ and $v(t)$ using the best fitness values for 5 number of neuron is shown in Fig 2. The absolute error (AE) is calculated for the parameters $x(t)$ and $w(t)$ in the first half of Fig. 3, while the AE for $y(t)$ and $v(t)$ is calculated in the second half of Fig. 3. The present results are compared with the Adams numerical scheme. It is clear in Fig. 3(a), that the AE for $x(t)$ and $w(t)$ lie in the ranges of 10^{-06} to 10^{-07}, while the AE for $y(t)$ and $v(t)$ lie around 10^{-05} to 10^{-07}. Fig. 4 shows the comparison of present results with the Adams numerical results using 5 number of neurons. The first portion of the Fig.

4 show the comparison for $x(t)$ and $w(t)$, while the second portion related the values of y(t) and $v(t)$ The overlapping of the present results with the Adams numerical results show the correctness and exactness of the present scheme. The performance measures along with the histograms of the statistical operators MAD, RMSE and TIC are narrated in Figs. 5 to 7. It is clear in understanding that more than 80% of independent executions attained best values of the statistical operators for MAD and RMSE. However, more than 90% of independent executions achieved best values for statistical operator TIC. The outclass performance of the designed algorithm is observed accurately and precisely in terms of statistical operators based on MAD, RMSE and TIC.

For precision analysis, statistical gages based on minimum (Min), Maximum (Max), median (Med) and semi interquartile range (SIR) are provided for the present technique. SIR is one-half of the difference of third quartile (Q_3=75% data) and first quartile (Q_1= 25% data). The statistical conclusions in Min, Max, Med and SIR gages for problem 1 are tabulated in Tables 2 for $x(t)$ and $w(t)$, while in Table 3 for $y(t)$ and $v(t)$. The scale of Min values for $x(t)$, $w(t)$, $y(t)$ and $v(t)$ lies around 10^{-07} to 10^{-09} for all neurons. However, the Med and SIR values for $x(t)$, $w(t)$, $y(t)$ and $v(t)$ are closer to 10^{-05}.

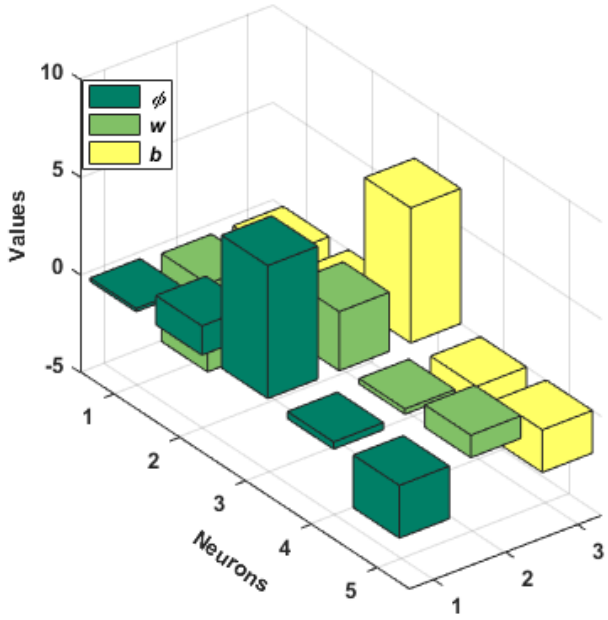

(a): Weights of 5 neurons for $x(t)$

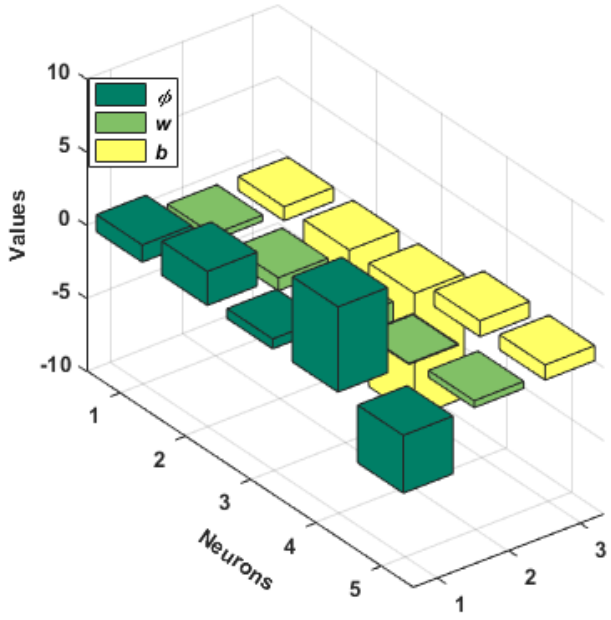

(b): Weights of 5 neurons for $w(t)$

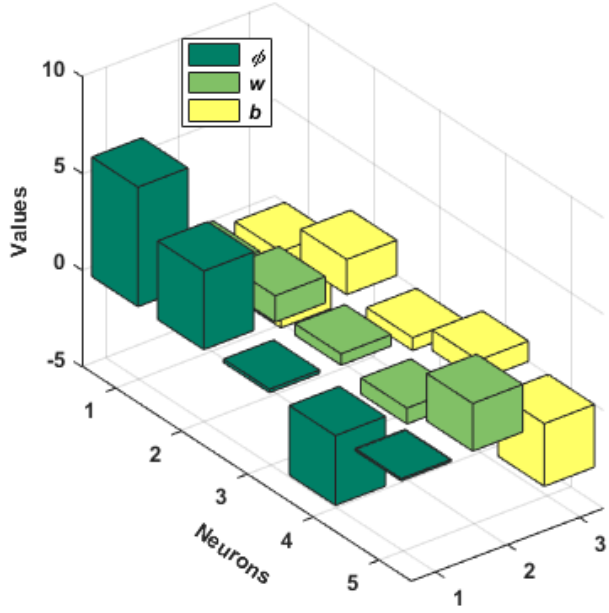

(c): Weights of 5 neurons for $y(t)$

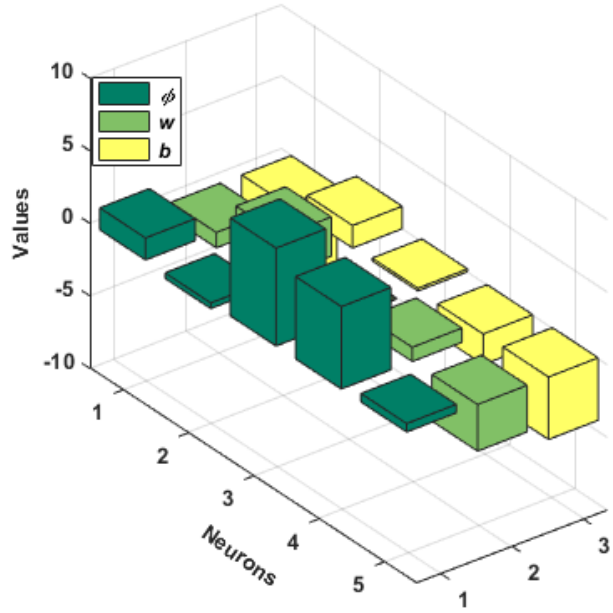

(d): Weights of 5 neurons for $v(t)$

Figure 2: A set of weights using best fitness for 5 neurons

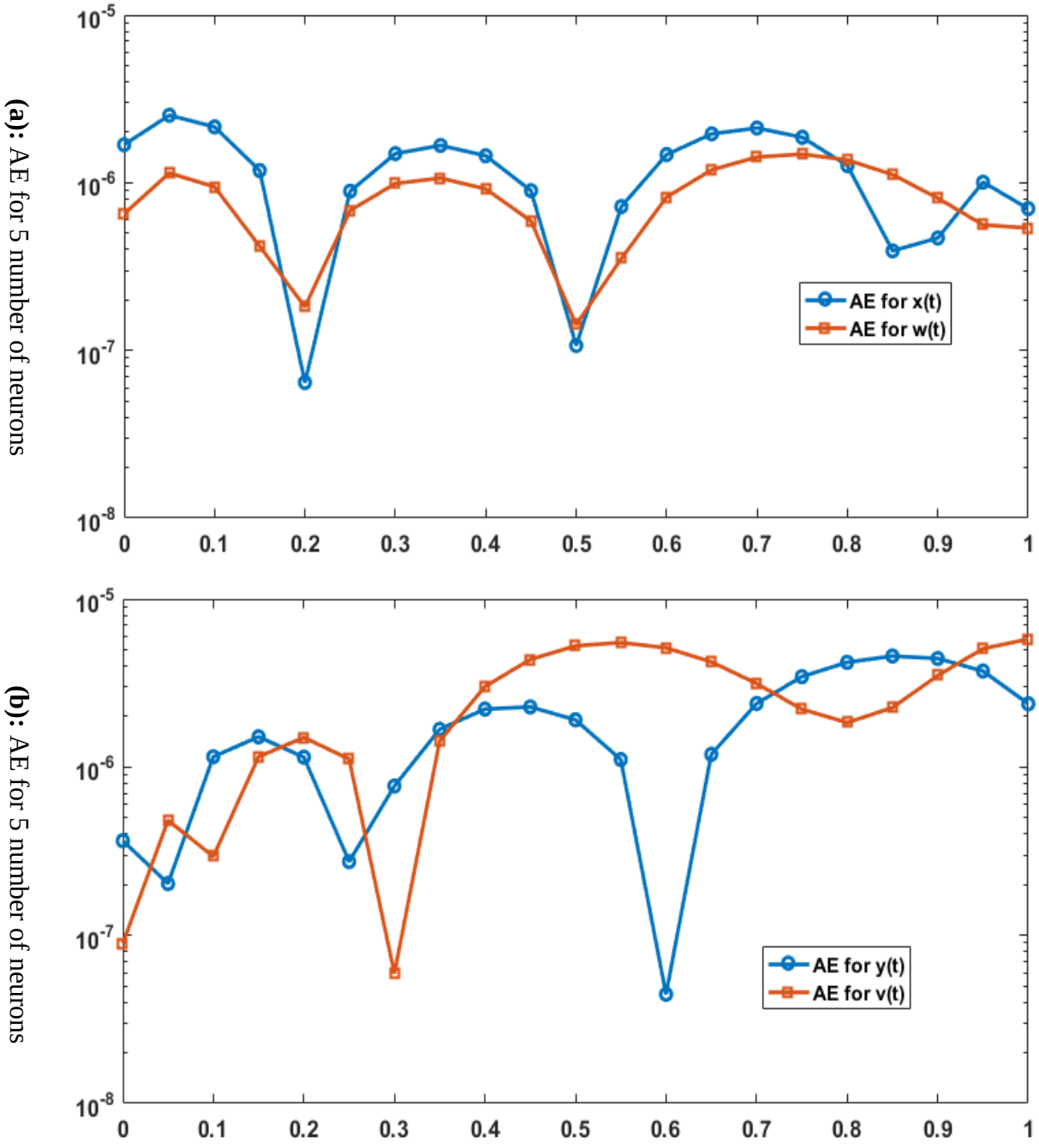

Figure 3: AE of the present results with the Adams results using 5 neurons

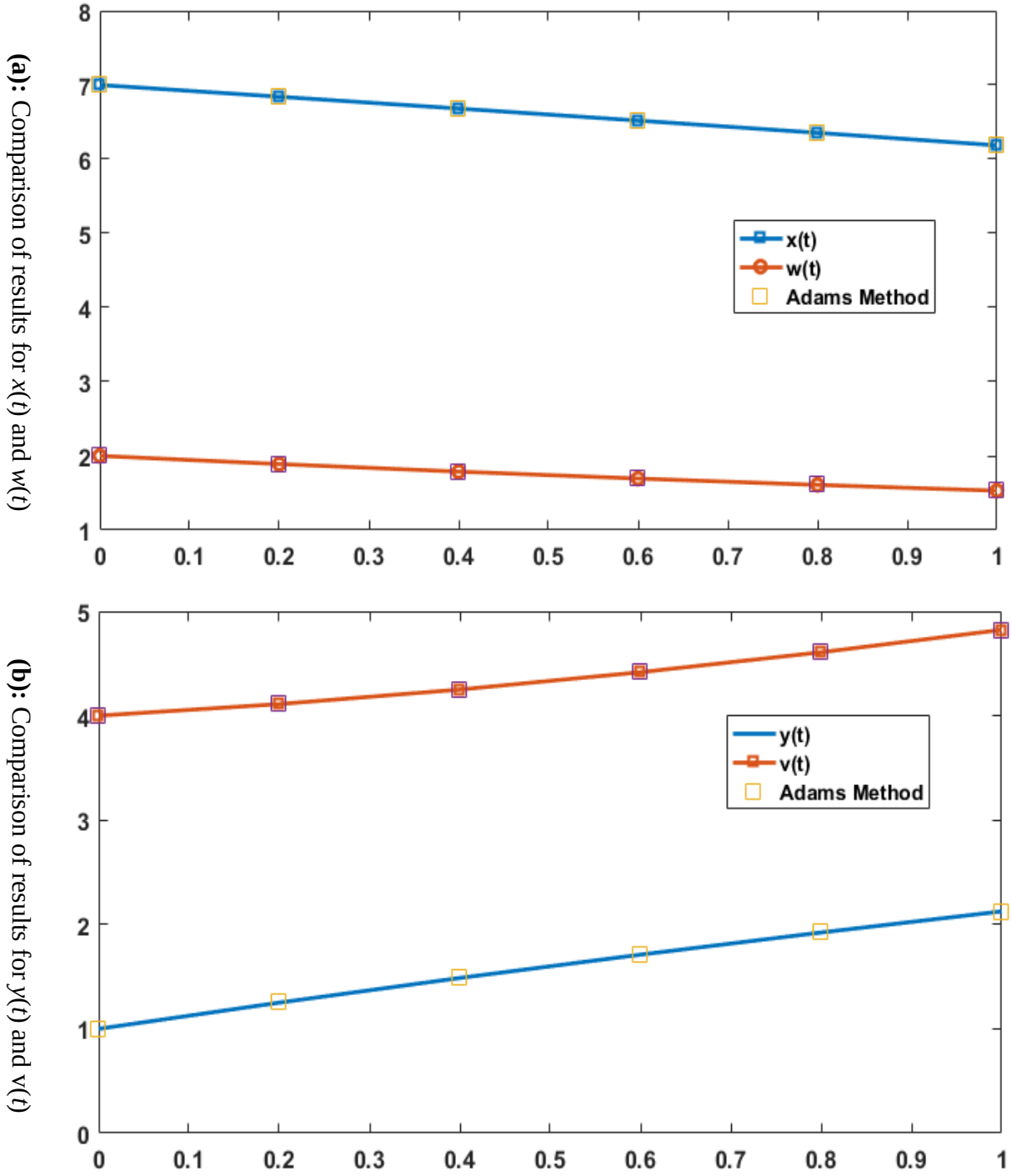

Figure 4: Comparison of present results with the Adams results using 5 neurons

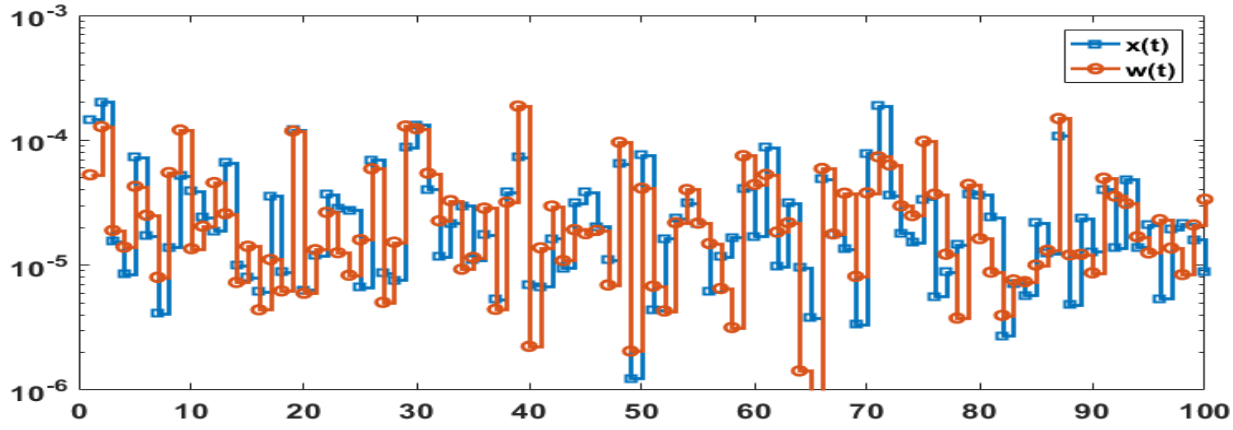

MAD value in convergence analysis for $x(t)$ and $w(t)$

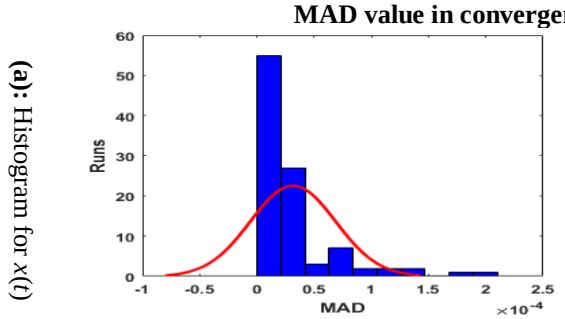

(a): Histogram for $x(t)$

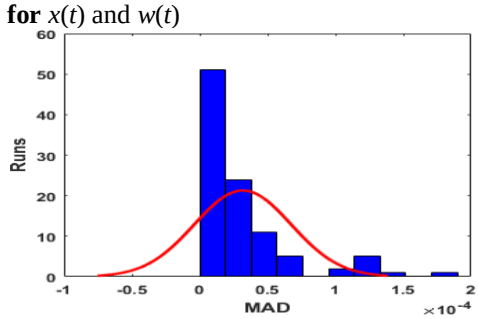

(c): Histogram for $w(t)$

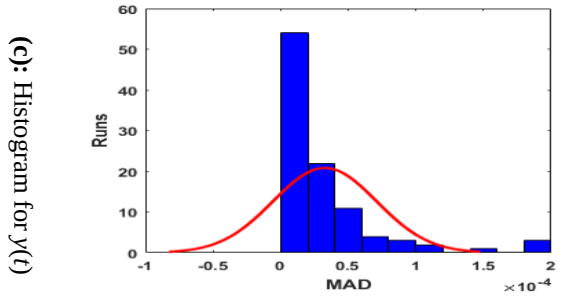

(c): Histogram for $y(t)$

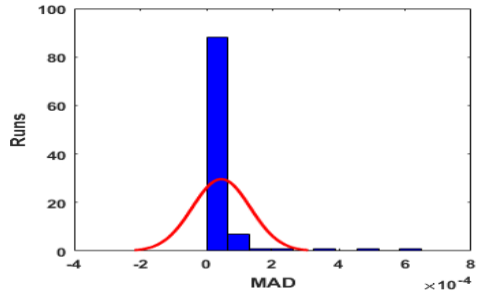

(d): Histogram for $v(t)$

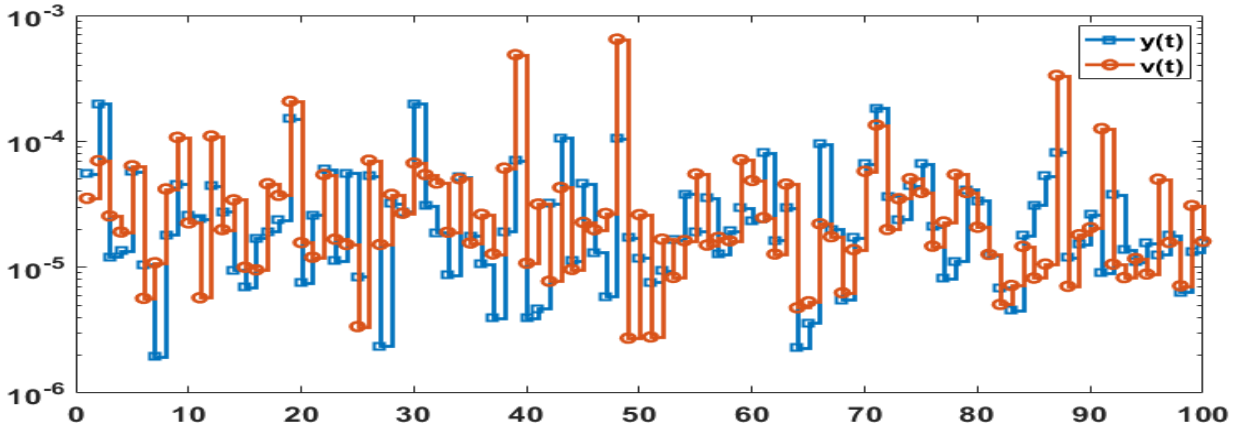

MAD value in convergence analysis for $y(t)$ and $v(t)$

Figure 5: MAD values in convergence analysis along with the histograms for 5 neurons

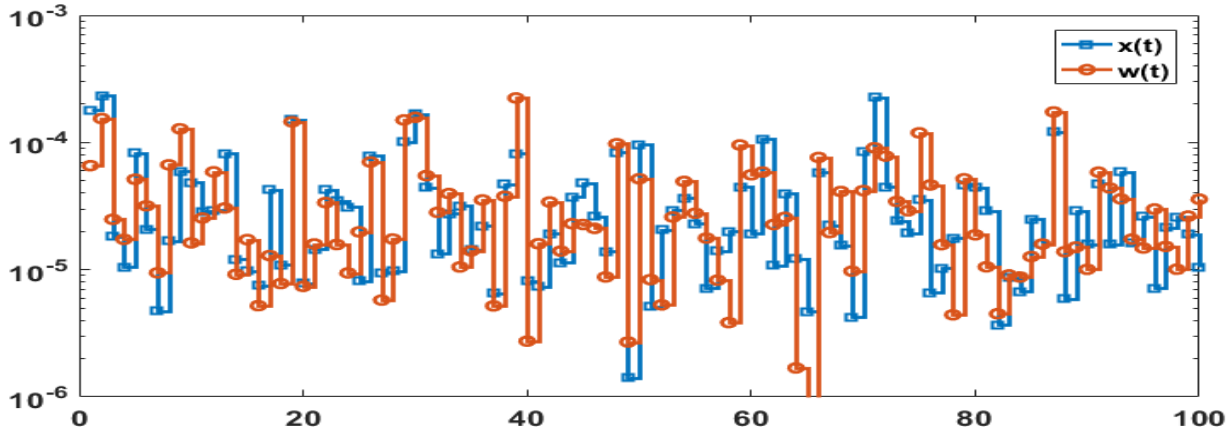

RMSE value in convergence analysis for $x(t)$ and $w(t)$

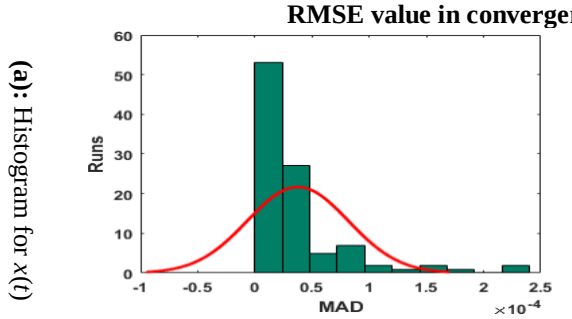

(a): Histogram for $x(t)$

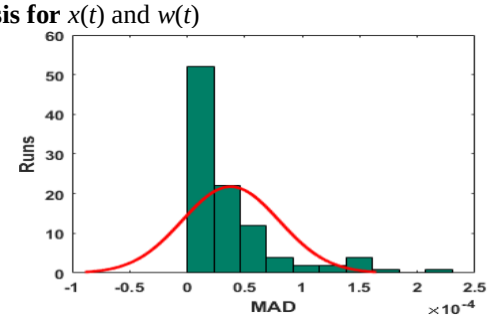

(c): Histogram for $w(t)$

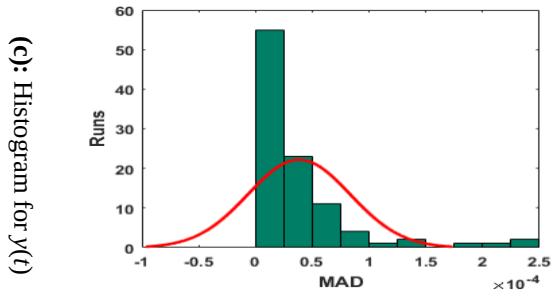

(c): Histogram for $y(t)$

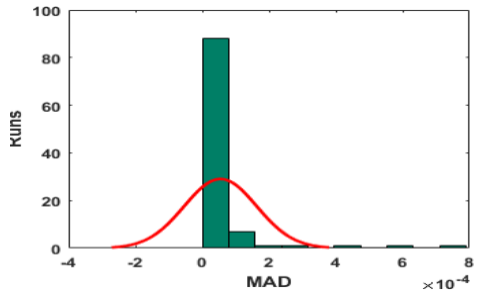

(d): Histogram for $v(t)$

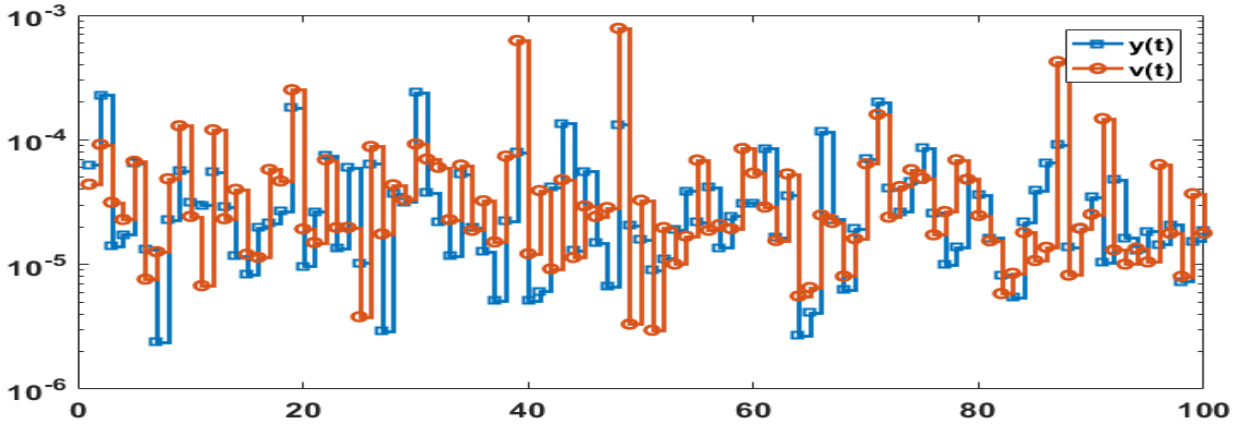

RMSE value in convergence analysis for $y(t)$ and $v(t)$

Figure 6: RMSE values in convergence analysis along with the histograms for 5 neurons

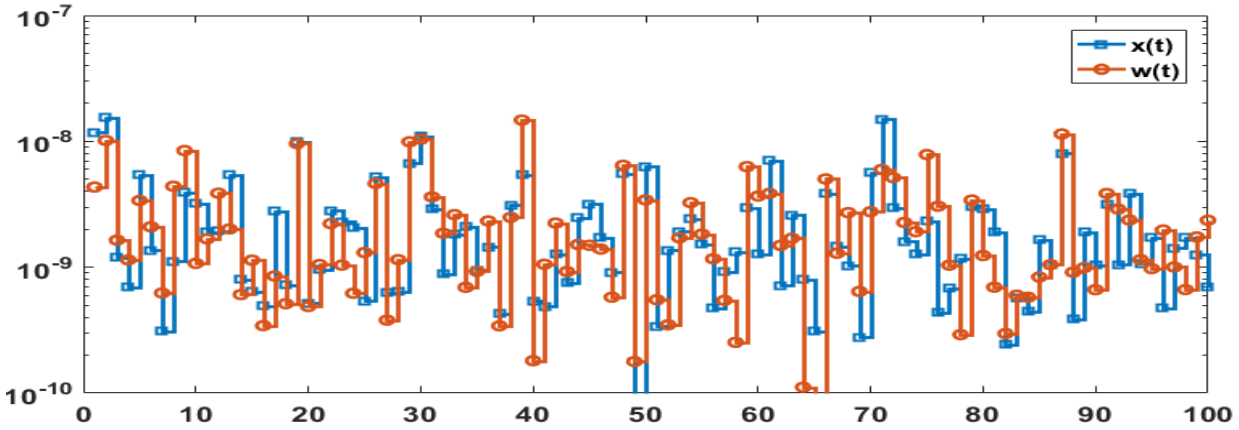

TIC value in convergence analysis for $x(t)$ and $w(t)$

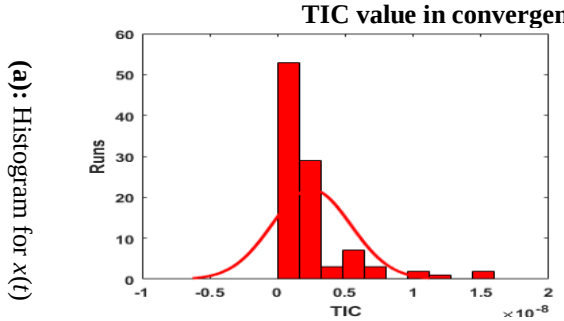

(a): Histogram for $x(t)$

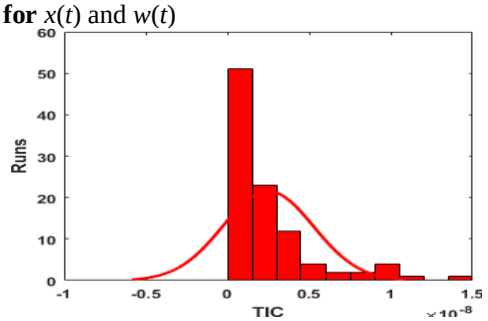

(c): Histogram for $w(t)$

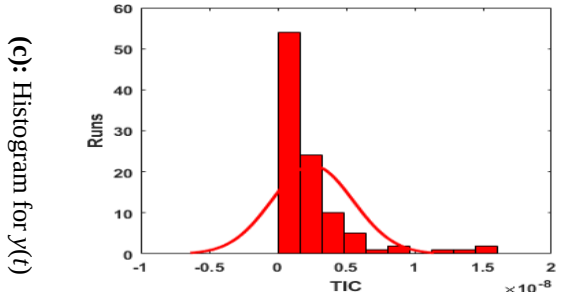

(c): Histogram for $y(t)$

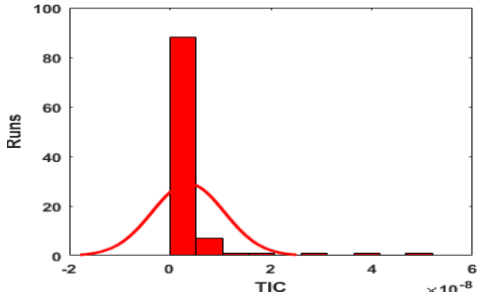

(d): Histogram for $v(t)$

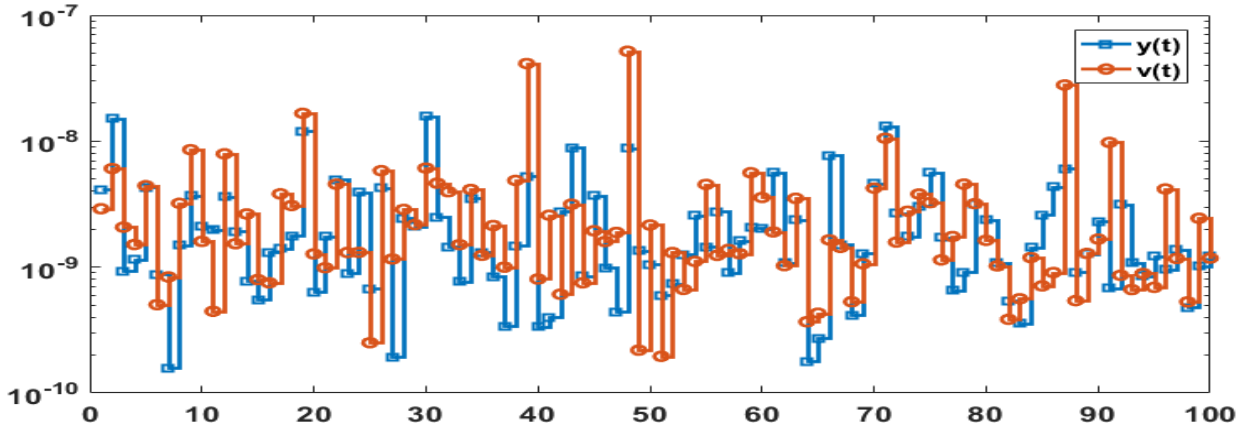

TIC value in convergence analysis for $y(t)$ and $v(t)$

Figure 7: TIC values in convergence analysis along with the histograms for 5 neurons

Table 2: Statistics based results of Problems 1 for $x(t)$ and $w(t)$

t	$x(t)$				$w(t)$			
	Min	**Max**	**Med**	**SIR**	**Min**	**Max**	**Med**	**SIR**
0	1.998E-08	1.301E-04	4.388E-06	6.397E-06	3.113E-09	1.301E-04	4.174E-06	6.611E-06
0.05	8.551E-08	1.589E-04	1.004E-05	1.259E-05	3.198E-08	1.589E-04	1.194E-05	1.105E-05
0.1	4.509E-08	2.279E-04	1.028E-05	1.091E-05	2.524E-07	2.279E-04	1.370E-05	1.140E-05
0.15	4.956E-08	2.215E-04	1.250E-05	1.275E-05	2.549E-07	2.215E-04	1.146E-05	9.729E-06
0.2	6.438E-08	1.616E-04	1.741E-05	1.377E-05	8.992E-08	1.616E-04	1.288E-05	8.493E-06
0.25	5.030E-08	1.457E-04	1.908E-05	1.661E-05	1.129E-07	1.457E-04	1.528E-05	1.087E-05
0.3	6.339E-07	2.105E-04	2.403E-05	1.841E-05	3.475E-07	2.105E-04	1.953E-05	1.562E-05
0.35	4.128E-07	2.715E-04	2.713E-05	2.136E-05	9.346E-07	2.715E-04	2.435E-05	2.053E-05
0.4	3.134E-07	3.223E-04	2.605E-05	2.174E-05	3.145E-07	3.223E-04	2.833E-05	2.512E-05
0.45	7.816E-07	3.581E-04	2.430E-05	2.454E-05	3.531E-08	3.581E-04	2.842E-05	2.762E-05
0.5	1.070E-07	3.890E-04	1.856E-05	2.195E-05	6.311E-08	3.890E-04	2.729E-05	2.849E-05
0.55	2.030E-07	4.076E-04	1.487E-05	2.009E-05	6.073E-08	4.076E-04	2.555E-05	2.452E-05
0.6	6.517E-07	3.911E-04	1.373E-05	1.531E-05	7.377E-08	3.911E-04	2.546E-05	1.906E-05
0.65	2.623E-07	3.407E-04	1.547E-05	1.306E-05	4.930E-08	3.407E-04	1.726E-05	1.391E-05
0.7	3.408E-07	2.740E-04	1.233E-05	1.005E-05	1.147E-07	2.740E-04	1.204E-05	1.102E-05
0.75	5.650E-08	2.213E-04	1.008E-05	1.004E-05	2.021E-08	2.213E-04	9.210E-06	1.332E-05
0.8	2.904E-07	2.258E-04	9.166E-06	1.047E-05	1.825E-08	2.258E-04	1.020E-05	1.194E-05
0.85	3.924E-07	2.711E-04	1.410E-05	1.356E-05	1.099E-07	2.711E-04	1.339E-05	1.223E-05
0.9	1.588E-07	2.945E-04	1.820E-05	1.706E-05	1.440E-08	2.945E-04	1.708E-05	1.337E-05
0.95	5.847E-07	2.877E-04	1.806E-05	1.426E-05	5.604E-07	2.877E-04	1.570E-05	1.293E-05
1	7.597E-08	2.424E-04	1.143E-05	1.062E-05	8.419E-08	2.424E-04	8.416E-06	7.541E-06

Table 3: Statistics based results of Problems 1 for $x(t)$ and $w(t)$

t	$x(t)$				$w(t)$			
	Min	**Max**	**Med**	**SIR**	**Min**	**Max**	**Med**	**SIR**
0	9.421E-08	1.301E-04	6.175E-06	1.030E-05	5.164E-08	1.301E-04	4.158E-06	4.250E-06
0.05	4.070E-08	1.589E-04	1.133E-05	1.555E-05	3.759E-08	1.589E-04	7.579E-06	9.194E-06
0.1	5.235E-08	2.279E-04	9.231E-06	1.404E-05	9.858E-08	2.279E-04	8.595E-06	8.275E-06
0.15	2.757E-08	2.215E-04	1.348E-05	1.372E-05	9.789E-08	2.215E-04	1.579E-05	1.522E-05
0.2	7.820E-07	1.616E-04	1.808E-05	1.286E-05	3.530E-07	1.616E-04	2.277E-05	1.817E-05
0.25	2.741E-07	1.457E-04	2.128E-05	1.488E-05	1.066E-06	1.457E-04	2.576E-05	2.443E-05
0.3	7.716E-07	2.105E-04	2.614E-05	1.637E-05	5.925E-08	2.105E-04	2.364E-05	2.975E-05
0.35	2.699E-07	2.715E-04	2.553E-05	1.442E-05	3.058E-07	2.715E-04	2.241E-05	2.937E-05
0.4	1.796E-07	3.223E-04	1.946E-05	1.608E-05	8.486E-08	3.223E-04	2.012E-05	2.138E-05
0.45	1.073E-07	3.581E-04	1.645E-05	1.803E-05	1.105E-07	3.581E-04	1.677E-05	1.496E-05
0.5	2.976E-08	3.890E-04	1.560E-05	1.612E-05	4.072E-08	3.890E-04	1.542E-05	1.166E-05
0.55	9.826E-08	4.076E-04	1.616E-05	1.606E-05	2.743E-08	4.076E-04	1.579E-05	1.458E-05
0.6	4.456E-08	3.911E-04	1.605E-05	1.441E-05	3.272E-07	3.911E-04	1.621E-05	1.618E-05
0.65	1.348E-07	3.407E-04	1.767E-05	1.548E-05	1.072E-07	3.407E-04	2.314E-05	1.614E-05
0.7	3.462E-07	2.740E-04	2.004E-05	1.229E-05	7.168E-07	2.740E-04	2.655E-05	1.684E-05
0.75	2.145E-07	2.213E-04	1.685E-05	1.397E-05	9.990E-07	2.213E-04	1.886E-05	1.466E-05
0.8	2.705E-08	2.258E-04	1.828E-05	1.671E-05	9.100E-08	2.258E-04	1.548E-05	1.373E-05
0.85	6.305E-07	2.711E-04	1.631E-05	1.796E-05	1.789E-07	2.711E-04	1.919E-05	1.709E-05
0.9	1.322E-07	2.945E-04	1.627E-05	1.598E-05	1.762E-07	2.945E-04	2.308E-05	2.153E-05
0.95	8.401E-07	2.877E-04	1.575E-05	1.348E-05	5.706E-07	2.877E-04	2.414E-05	1.856E-05
1	3.167E-07	2.424E-04	1.499E-05	1.057E-05	2.620E-07	2.424E-04	1.648E-05	1.235E-05

4. Conclusion

Some concluding remarks of the present scheme are as follows:

- A novel computing arrangement is designed for solving nonlinear biological HIV infection model of latently infected cells using artificial neural network optimized by global capabilities of particle swarm optimization and smartness of local search with interior-programming algorithm.
- The accuracy of the performance of present scheme is established by overlapping the Adams results up to 4–6 decimal places which proves the exactness for the designed scheme.
- The magnitudes of median and semi interquartile range calculated for 100 self-directed executions for a biological nonlinear HIV model that indicate the trustworthiness, steady and accurateness of the algorithm.
- Numerical and graphical graphics of performance indices of MAD, RMSE and TIC authenticate the correctness, stability and reliability of the present scheme.

References

[1] Rosenberg, E.S., Altfeld, M., Poon, S.H., Phillips, M.N., Wilkes, B.M., Eldridge, R.L., Robbins, G.K., Richard, T.D., Goulder, P.J. and Walker, B.D., 2000. Immune control of HIV-1 after early treatment of acute infection. Nature, 407(6803), p.523.

[2] Perelson, A.S., 1989. Modeling the interaction of the immune system with HIV. In Mathematical and statistical approaches to AIDS epidemiology (pp. 350-370). Springer, Berlin, Heidelberg.

[3] Perelson, A.S., Kirschner, D.E. and De Boer, R., 1993. Dynamics of HIV infection of CD4+ T cells. Mathematical biosciences, 114(1), pp.81-125.

[4] Ali, N. and Zaman, G., 2016. Asymptotic behavior of HIV-1 epidemic model with infinite distributed intracellular delays. SpringerPlus, 5(1), p.324.

[5] Wang, L. and Li, M.Y., 2006. Mathematical analysis of the global dynamics of a model for HIV infection of CD4+ T cells. Mathematical Biosciences, 200(1), pp.44-57.

[6] Ali, N., Zaman, G. and Algahtani, O., 2016. Stability analysis of HIV-1 model with multiple delays. Advances in Difference Equations, 2016(1), p.88.

[9] Adomian, G., 1991. Solving frontier problems modelled by nonlinear partial differential equations. Computers & Mathematics with Applications, 22(8), pp.91-94.

[10] Ali, N., Ahmad, S., Aziz, S. and Zaman, G., 2019. The Adomian Decomposition Method For Solving Hiv Infection Model Of Latently Infected Cells. Matrix Science Mathematic (MSMK), 3(1), pp.5-8.

[11] Zibaei, S.A.D.E.G.H. and Namjoo, M.I.E.H.R.A.N., 2015. A nonstandard finite difference scheme for solving fractional-order model of HIV-1 infection of CD4^{+} t-cells. Iranian Journal of Mathematical Chemistry, 6(2), pp.169-184.

[12] Venkatesh, S.G., Balachandar, S.R., Ayyaswamy, S.K. and Balasubramanian, K., 2016. A new approach for solving a model for HIV infection of $$\mathbf {CD4}^{+}\,\mathbf {T} $$-cells arising in mathematical chemistry using wavelets. Journal of Mathematical Chemistry, 54(5), pp.1072-1082.

[13] Prague, M., 2016. Use of dynamical models for treatment optimization in HIV infected patients: a sequential Bayesian analysis approach.

[14] Ghoreishi, M., Ismail, A.M. and Alomari, A.K., 2011. Application of the homotopy analysis method for solving a model for HIV infection of CD4+ T-cells. Mathematical and Computer Modelling, 54(11-12), pp.3007-3015.

[15] Yüzbaşı, Ş., 2012. A numerical approach to solve the model for HIV infection of CD4+ T cells. Applied Mathematical Modelling, 36(12), pp.5876-5890.

[16] Srivastava, V.K., Awasthi, M.K. and Kumar, S., 2014. Numerical approximation for HIV infection of CD4+ T cells mathematical model. Ain Shams Engineering Journal, 5(2), pp.625-629.

[17] Kumar, M. and Yadav, N., 2015. Numerical solution of Bratu's problem using multilayer perceptron neural network method. National Academy Science Letters, 38(5), pp.425-428.

[18] Aidara, S., 2019. Anticipated backward doubly stochastic differential equations with non-Liphschitz coefficients. Applied Mathematics and Nonlinear Sciences, 4(1), pp.9-20.

[19] Yadav, N., Yadav, A., Kumar, M. and Kim, J.H., 2017. An efficient algorithm based on artificial neural networks and particle swarm optimization for solution of nonlinear Troesch's problem. Neural Computing and Applications, 28(1), pp.171-178.

[20] Chen, H., Jiang, J., Cao, D. and Fan, X., 2018. Numerical investigation on global dynamics for nonlinear stochastic heat conduction via global random attractor's theory. Applied Mathematics and Nonlinear Sciences, 3(1), pp.175-186.

[21] Motyl, J., 2017. Upper separated multifunctions in deterministic and stochastic optimal control. Applied Mathematics and Nonlinear Sciences, 2(2), pp.479-484.

[22] Umar, M., Sabir, Z. and Raja, M.A.Z., 2019. Intelligent computing for numerical treatment of nonlinear prey–predator models. Applied Soft Computing, 80, pp.506-524.

[23] Raja, M.A.Z., Shah, F.H., Tariq, M. and Ahmad, I., 2018. Design of artificial neural network models optimized with sequential quadratic programming to study the dynamics of nonlinear Troesch's problem arising in plasma physics. Neural Computing and Applications, 29(6), pp.83-109.

[24] Schaff, J.C., Gao, F., Li, Y., Novak, I.L. and Slepchenko, B.M., 2016. Numerical approach to spatial deterministic-stochastic models arising in cell biology. PLoS computational biology, 12(12), p.e1005236.

[25] Momani, S., Abo-Hammour, Z.S. and Alsmadi, O.M., 2016. Solution of inverse kinematics problem using genetic algorithms. Applied Mathematics & Information Sciences, 10(1), p.225.
[26] Raja, M.A.Z., Khan, J.A. and Haroon, T., 2015. Stochastic numerical treatment for thin film flow of third grade fluid using unsupervised neural networks. Journal of the Taiwan Institute of Chemical Engineers, 48, pp.26-39.
[27] Soize, C., 2012. Stochastic models of uncertainties in computational structural dynamics and structural acoustics. In Nondeterministic Mechanics (pp. 61-113). Springer, Vienna.
[28] Pelletier, F., Masson, C. and Tahan, A., 2016. Wind turbine power curve modelling using artificial neural network. Renewable Energy, 89, pp.207-214.
[29] Effati, S. and Pakdaman, M., 2010. Artificial neural network approach for solving fuzzy differential equations. Information Sciences, 180(8), pp.1434-1457.
[30] Raja, M.A.Z., Farooq, U., Chaudhary, N.I. and Wazwaz, A.M., 2016. Stochastic numerical solver for nanofluidic problems containing multi-walled carbon nanotubes. Applied Soft Computing, 38, pp.561-586.
[31] Sabir, Z., Manzar, M.A., Raja, M.A.Z., Sheraz, M. and Wazwaz, A.M., 2018. Neuro-heuristics for nonlinear singular Thomas-Fermi systems. Applied Soft Computing, 65, pp.152-169.
[32] Raja, M.A.Z., Mehmood, J., Sabir, Z., Nasab, A.K. and Manzar, M.A., 2019. Numerical solution of doubly singular nonlinear systems using neural networks-based integrated intelligent computing. Neural Computing and Applications, 31(3), pp.793-812.
[33] Raja, M.A.Z., Umar, M., Sabir, Z., Khan, J.A. and Baleanu, D., 2018. A new stochastic computing paradigm for the dynamics of nonlinear singular heat conduction model of the human head. The European Physical Journal Plus, 133(9), p.364.
[34] Zhang, Z., El-Moselhy, T.A., Elfadel, I.M. and Daniel, L., 2013. Stochastic testing method for transistor-level uncertainty quantification based on generalized polynomial chaos. IEEE Transactions on Computer-Aided Design of Integrated Circuits and Systems, 32(10), pp.1533-1545.
[35] He, W., Chen, Y. and Yin, Z., 2015. Adaptive neural network control of an uncertain robot with full-state constraints. IEEE transactions on cybernetics, 46(3), pp.620-629.
[36] Deb, C., Eang, L.S., Yang, J. and Santamouris, M., 2016. Forecasting diurnal cooling energy load for institutional buildings using Artificial Neural Networks. Energy and Buildings, 121, pp.284-297.
[37] Shi, Y. and Eberhart, R. C., 1999. Empirical study of particle swarm optimization. In Proceedings of the 1999 Congress on Evolutionary Computation-CEC99 (Cat. No. 99TH8406) (Vol. 3, pp. 1945-1950). IEEE.
[38] Engelbrecht, A. P., 2007. Computational intelligence: an introduction. John Wiley & Sons.
[39] Shi, Y., 2001. Particle swarm optimization: developments, applications and resources. In Proceedings of the 2001 Congress on Evolutionary Computation (IEEE Cat. No. 01TH8546) (Vol. 1, pp. 81-86). IEEE.
[40] Shen, M., Zhan, Z. H., Chen, W. N., Gong, Y. J., Zhang, J. and Li, Y., 2014. Bi-velocity discrete particle swarm optimization and its application to multicast routing problem in communication networks. IEEE Transactions on Industrial Electronics, 61(12), pp.7141-7151.
[41] Khare, A. and Rangnekar, S., 2013. A review of particle swarm optimization and its applications in solar photovoltaic system. Applied Soft Computing, 13(5), pp.2997-3006.
[42] Esmin, A. A., Coelho, R. A. and Matwin, S., 2015. A review on particle swarm optimization algorithm and its variants to clustering high-dimensional data. Artificial Intelligence Review, 44(1), pp.23-45.
[43] Akay, B., 2013. A study on particle swarm optimization and artificial bee colony algorithms for multilevel thresholding. Applied Soft Computing, 13(6), pp.3066-3091.
[44] Soares, J., Sousa, T., Morais, H., Vale, Z., Canizes, B. and Silva, A., 2013. Application-Specific Modified Particle Swarm Optimization for energy resource scheduling considering vehicle-to-grid. Applied Soft Computing, 13(11), pp.4264-4280.
[45] Lee, K. B. and Kim, J. H., 2013. Multiobjective particle swarm optimization with preference-based sort and its application to path following footstep optimization for humanoid robots. IEEE Transactions on Evolutionary Computation, 17(6), pp.755-766.
[46] Doctor, S., Venayagamoorthy, G. K. and Gudise, V. G., 2004, June. Optimal PSO for collective robotic search applications. In Proceedings of the 2004 Congress on Evolutionary Computation (IEEE Cat. No. 04TH8753) (Vol. 2, pp. 1390-1395). IEEE

[47] Alba, E., Garcia-Nieto, J., Jourdan, L. and Talbi, E. G., 2007, September. Gene selection in cancer classification using PSO/SVM and GA/SVM hybrid algorithms. In 2007 IEEE Congress on Evolutionary Computation (pp. 284-290). IEEE.

[48] Kardos, J., Kourounis, D., Schenk, O. and Zimmerman, R., 2018. Complete results for a numerical evaluation of interior point solvers for large-scale optimal power flow problems. arXiv preprint arXiv:1807.03964.

[49] Stefanova, M., Yakunin, S., Petukhova, M., Lupuleac, S. and Kokkolaras, M., 2018. An interior-point method-based solver for simulation of aircraft parts riveting. Engineering Optimization, 50(5), pp.781-796.

[50] Bleyer, J., 2018. Advances in the simulation of viscoplastic fluid flows using interior-point methods. Computer Methods in Applied Mechanics and Engineering, 330, pp.368-394.

[51] Raja, M.A.Z., Ahmed, U., Zameer, A., Kiani, A.K. and Chaudhary, N.I., 2019. Bio-inspired heuristics hybrid with sequential quadratic programming and interior-point methods for reliable treatment of economic load dispatch problem. Neural Computing and Applications, 31(1), pp.447-475.

[52] Mangoni, D., Tasora, A. and Garziera, R., 2018. A primal–dual predictor–corrector interior point method for non-smooth contact dynamics. Computer Methods in Applied Mechanics and Engineering, 330, pp.351-367.